Liquid Crystals
Publication details, including instructions for authors and subscription information:
http://www.informaworld.com/smpp/title~content=t713926090

TGB_A phase in a series of propionates containing two stereocenters

Shung-Long Wu[a]; Wen-Jiunn Hsieh[a]
[a] Department of Chemical Engineering, Tatung Institute of Technology, Taipei, Taiwan, R.O.C.

To cite this Article Wu, Shung-Long and Hsieh, Wen-Jiunn(1996) 'TGB_A phase in a series of propionates containing two stereocenters', Liquid Crystals, 21: 6, 783 — 790
To link to this Article: DOI: 10.1080/02678299608032894
URL: http://dx.doi.org/10.1080/02678299608032894

LIQUID CRYSTALS, 1996, VOL. 21, NO. 6, 783–790

TGB_A^* phase in a series of propionates containing two stereocenters

by SHUNG-LONG WU* and WEN-JIUNN HSIEH
Department of Chemical Engineering, Tatung Institute of Technology, Taipei 10451, Taiwan, R.O.C.

(*Received 12 April 1996; in final form 14 August 1996; accepted 14 August 1996*)

A homologous series of chiral materials, (*R*)-2-pentyl (*S*)-2-(6-(4-(4′-alkoxyphenyl)benzoyloxy)-2-naphthyl)propionates (*R,S*)P*m*PBNP (*m* = 7–14), derived from a naphthalene ring as part of the core structure in conjunction with a chiral tail containing two stereocentres has been synthesized for the investigation. The twist grain boundary smectic A* (TGB_A^*) and smectic C* (TGB_C^*) phases were characterized by the microscopic textures of compounds packed in two untreated glass slides, Cano wedge cell, or homogeneously aligned cell. It was found that the occurrence of these phases depend remarkably on the nature of alkyl chain length *m*; in the case of shorter alkyl chain length (*m* = 7–10), the TGB_A^* phase behaves as a metastable-like phase mediated between N* and S_A^* phases in a short temperature range, whereas in the longer chain length (*m* = 11–14), both the TGB_A^* and TGB_C^* phases become thermodynamically stable phases with a wide temperature range. Consequently, this series of chiral materials resulted in two different mesophase sequences: N*–TGB_A^*–S_A^*–S_C^* and N*–TGB_A^*–TGB_C^*. A kind of parquet texture displaying two types of domain with different relative directions of the smectic layer normal was found in the S_C^* phase from the materials (*m* = 9–14) packed in 2 μm homogeneously aligned cells and cooled down from the isotropic liquid without applying an electric field. The magnitudes of spontaneous polarization (P_s) in the S_C^* and TGB_C^* phases showed that the P_s values are nearly the same for all compounds at the same temperature below the Curie point. Dielectric measurements revealed no significant occurrence of soft mode switching in the TGB_A^* phase.

1. Introduction

The discovery of twist grain boundary phases: TGB_A^*, TGB_C and TGB_C^* phases in chiral liquid crystalline systems [1–4], has stimulated a great interest in investigating these new types of materials. The structural designs for the studies, however, were limited and mainly based on the first series of chiral materials, 1-methylheptyl 4′-[(4-alkoxyphenyl)propioloyloxy]biphenyl-4-carboxylates, that revealed a TGB_A^* phase [1]. Thus, the core structures of the materials generally found were propiolate esters [1, 4–6], tolane esters [3, 7] and esters of structurally similar homologues [8, 9] composed of three benzene rings. A recent report showed that the cinnamoate esters composed of two benzene rings also exhibited a TGB_A^* phase [10]. Amongst them, chiral groups connected to the core that promote the formation of helical or twisted phases were optically active alkan-2-ols, lactic acid, and α-halohydrines that were derived from L-amino acids. The correlation of molecular structure to the appearance of TGB phases was reviewed [11] herein.

In this paper, we report for the first time a new series of chiral materials with totally different molecular structures that exhibit a TGB_A^* phase. This series, (*R*)-2-pentyl (*S*)-2-(6-(4-(4′-alkoxyphenyl)benzoyloxy)-2-naphthyl)-propionates, (*R,S*)P*m*PBNP (*m* = 7–14), contains a naphthalene ring as part of the core structure in conjunction with a chiral tail containing two stereocentres and has the general formula:

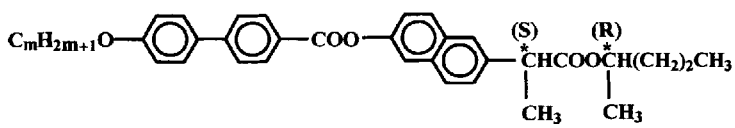

*Author for correspondence.

0267–8292/96 $12·00

The influence of the alkyl chain length on the formation and stability of the TGB_A^* and TGB_C^* phases, and some physical properties such as spontaneous polarization, and the dielectric permittivity of the S_C^* phase are also presented and discussed.

2. Experimental

2.1. *Characterization of materials*

The chemical structures for all materials prepared were analysed by nuclear magnetic resonance (NMR) spectroscopy using a JEOL EX-400 FT-NMR spectrometer. The purity of the final compounds was checked by thin layer chromatography. Further confirmation for the purity was performed by elemental analysis using a Perkin–Elmer 2400 spectrometer. The magnitudes of specific rotations were measured in dichloromethane using a JASCO DIP-360 digital polarimeter. Transition temperatures and heats of transitions were determined by differential scanning calorimetry (DSC) using a DuPont DSC-910 calorimeter at a running rate of $2°C\,min^{-1}$. Mesophases were identified by observing the textures using a Nikon Microphot-FXA optical microscope under crossed polarizers with a Mettler FP82-HT hot stage in connection with a Mettler FP80-HT heat controller. The magnitudes of spontaneous polarization (P_s) of the S_C^* phase were measured by the triangular wave method [12] with the frequency of 100 Hz and the amplitude of $38{\cdot}5\,V_{p-p}$. The dielectric measurements were carried out using a HP4284A precision LCR meter (20 Hz–1 MHz) with a Lakeshore DRC-93CA temperature controller at the heating and cooling rate of $0{\cdot}5°C\,min^{-1}$ with a temperature accuracy of $\pm 0{\cdot}01°C$. The homogeneously aligned liquid crystal sample cells with 5 μm cell gap and $0{\cdot}25\,cm^2$ conducting area were purchased from Linkam Scientific Instruments Ltd., UK. The sample cells with 25 μm cell gap and $0{\cdot}25\,cm^2$ electrode area were purchased from E.H.C. Co., Japan.

2.2. *Preparation of materials*

The chiral starting material for the synthesis of the compounds (*R,S*)P*m*PBNP is (*S*)-2-(6-methoxy-2-naphthyl)propionic acid, purchased from Tokyo Chemical Industry (TCI) Co. Ltd., with optical purity greater than 99 per cent enantiomeric excess. The synthetic procedures were carried out in the same manner as described previously [13] and are shown in the scheme. The acid **1** was esterified with (*R*)-2-pentanol in the presence of *N,N'*-dicyclohexyl carbodiimide (DCC) and 4-dimethylaminopyridine (DMAP) to produce the ester, (*R*)-2-pentyl (*S*)-2-(6-methoxy-2-naphthyl)propionate **Ia**. The methoxy group of this ester was demethylated by treatment with tribromoborane (BBr_3), and the resulting hydroxy group of (*R*)-2-pentyl (*S*)-2-(6-hydroxy-2-naphthyl)propionate **Ib** was subsequently esterified with a variety of 4-(4'-alkoxyphenyl)benzoic acids **2** by the treatment of DCC and DMAP to produce the target compounds. The synthetic details of these compounds are described below.

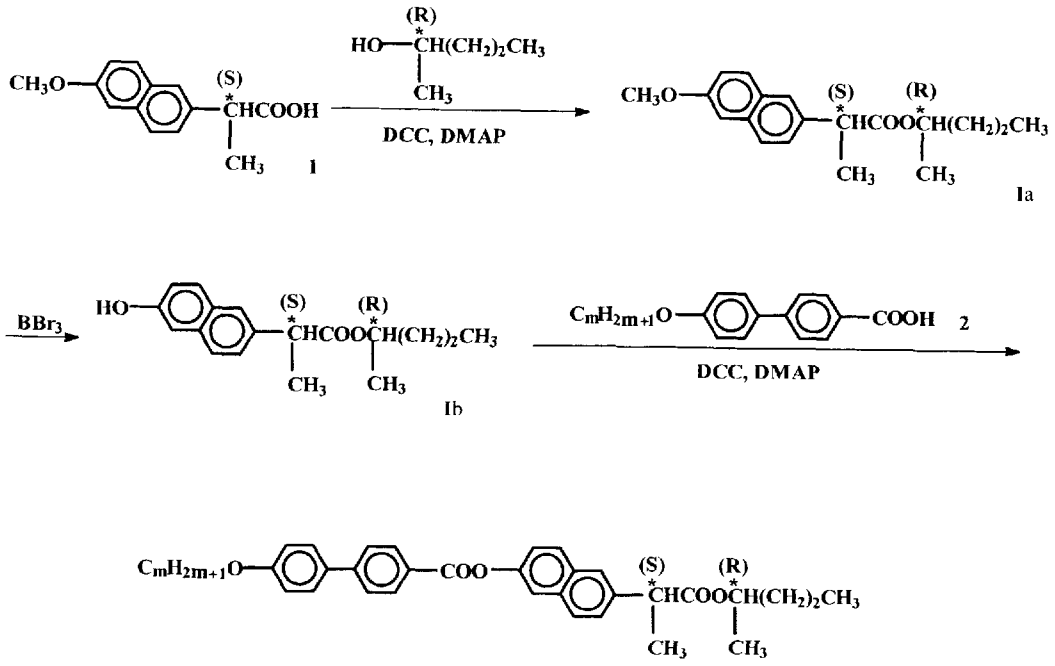

Scheme. Mechanistic procedures for the synthesis of compounds (*R*)-2(6-(4-(4'-alkoxyphenyl)benzoyloxy)-2'-naphthyl)propionates.

2.2.1. *(R)-2-Pentyl (S)-2-(methoxy-2-naphthyl)propionates, Ia*

The (S)-2-(6-methoxy-2-naphthyl)propionic acid (25 mmol) and (R)-2-pentanol (27·5 mmol) were dissolved in dry dichloromethane (100 ml). After the addition of DCC (27·5 mmol) and DMAP (2·5 mmol), the solution was stirred at room temperature for 5 d. The precipitates were filtrated and washed with dichloromethane. The filtrate was successively washed with 5 per cent acetic acid, 5 per cent aqueous sodium hydroxide and water, dried over anhydrous magnesium sulphate, and concentrated in vacuum. The residue was purified by column chromatography over silica gel (70–230 mesh) with dichloromethane as eluent. The product **Ia** was obtained with the yield of 84 per cent and used directly without further purification. ^{1}H NMR ($CDCl_3$): δ (ppm) 0·7–1·7 (m, 13 H), 3·8 (q, 1 H), 3·9 (s, 3 H), 4·9–5·0 (m, 1 H), 7·0–7·7 (m, 6 H).

2.2.2. *(R)-2-Pentyl (S)-2-(6-hydroxy-2-naphthyl)propionoates, Ib*

To the ester **Ia** (4·5 g, 0·015 mol) dissolved in dry dichloromethane (57 ml) was added BBr_3 (2·5 ml) at −20°C. The mixture was stirred at −20°C for 5 min, and at 0°C for 50 min. After diluting with dichloromethane (117 ml), the solution was poured into a mixture of saturated ammonium chloride (57 ml) and crushed ice (53 g), the organic layer was separated and washed with brine–ice, dried over anhydrous sodium sulphate, and concentrated in vacuum. The residue was purified by column chromatography over silica gel (70–230 mesh) using dichloromethane as eluent. The alcohol **Ib** was collected after recrystallization from hexane with a yield of 73 per cent. Elemental analysis (per cent): calculated, C 75·48, H 7·75; found, C 75·34, C 7·64. ^{1}H NMR ($CDCl_3$): δ (ppm) 0·8–1·6 (m, 13 H), 3·8 (q, 1 H), 4·9–5·0 (m, 1 H), 6·3 (s, 1 H), 7·0–7·7 (m, 6 H).

2.2.3. *(R)-2-Pentyl (S)-2-(6-(4-(4'-alkoxyphenyl)benzoyloxy)-2-naphthyl)propionates, (R,S)PmPBNP*

A mixture of 4-(4'-alkoxyphenyl)benzoic acids **2** (1·16 mmol), alcohol **Ib** (1·05 mmol), DCC (1·26 mmol), and dry tetrahydrofuran (3 ml) was stirred at room temperature for 5 d. The precipitates were filtrated and washed with dichloromethane. The filtrate was successively washed with 5 per cent acetic acid, 5 per cent aqueous sodium hydroxide and water, dried over anhydrous sodium sulphate, and concentrated in vacuum. The residue was purified by column chromatography over silica gel (70–230 mesh) using dichloromethane as eluent. The esters (R,S)P*m*PBNP were collected after recrystallization from absolute alcohol with yields of 63–90 per cent. All materials were identified in a satisfactory results. Typical example of (R,S)P12PBNP is given as follows: Elemental analysis (per cent): calculated, C 79·35, H 8·37; found, C 78·96, H 8·36. ^{1}H NMR ($CDCl_3$); δ (ppm) 0·1–1·9 (m, 36 H), 3·8–3·9 (q, 1 H), 4·0–4·1 (t, 2 H), 4·9–5·0 (m, 1 H), 7·1–8·3 (m, 14 H). Specific rotation, $[\alpha]_D^{25·6} = -0·61°$ (*c* 0·620 g 100ml^{-1}).

3. Results and discussion

3.1. *Transition temperatures and mesophases*

The mesophase transition temperatures for materials (R,S)P*m*PBNP were determined by DSC in conjunction with optical microscopy. Mesophase identification was carried out principally by observing the microscopic textures of the materials sandwich-packed between the untreated glass plates. Ferroelectric S_C^* phases were further characterized by other electro-optical methods [14].

Representative DSC thermograms for compounds (R,S)P*m*PBNP (*m* = 9 and 12) are depicted in figure 1 on cooling. Figure 1 (*a*) refers to the cooling trace of (R,S)P9PBNP indicating that, as the temperature is lowered from the isotropic liquid (I), the phase transition occurs initially from the I to N* phase at 142·8°C, and subsequently to the TGB_A^* phase at 140·8°C. A significant transition of the TGB_A^* to the S_A^* phase appears at the shoulder of the exothermic peak of the N* to S_A^* transition, demonstrating that the TGB_A^* phase is mediated between the transition of N* and S_A^* phases in a short temperature range as predicted by De Gennes [15] and Lubensky and Renn [16] due to pretransitional effects. Similar thermal traces are also observed for the compounds with shorter alkyl chain lengths (*m* = 7, 8 and 10). It is seen, however, that there is a slightly different DSC pattern in figure 1 (*b*) obtained for compound (R,S)P12PBNP. On cooling from the isotropic liquid, the I–N* transition occurs at 132·6°C, and is then followed by the N*–TGB_A^* transition at 126·4°C. On continuously lowering the temperature, the TGB_A^* phase range remains as wide as 13°C and is subsequently transformed to the TGB_C^* phase at 113·4°C and remains until crystallization. These thermodynamically stable TGB_A^* and TGB_C^* phases are also found in the compounds with longer alkyl chain lengths (*m* = 11, 13 and 14). All mesophases detected are enantiotropic.

The resulting mesophases and their corresponding transition temperatures are listed in the table. The phase behaviour of the (R,S)P*m*PBNP series as a function of the alkyl chain length *m*, is plotted in figure 2. It is clearly shown that the transition temperatures for both the N*–TGB_A^* and TGB_A^*–S_A^* transitions gradually decrease, however, the temperature ranges of the TGB_A^* phase increase from 1·3°C to 5·6°C as *m* increases from 7 to 10, correspondingly. The decline of the N*–TGB_A^* transition temperatures accompanied with the

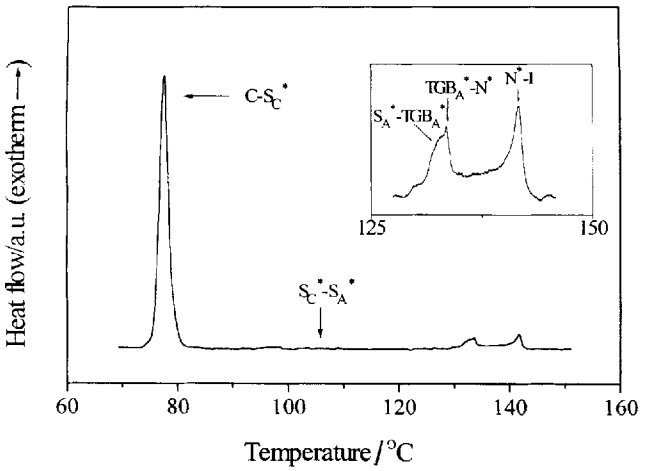

(*a*)

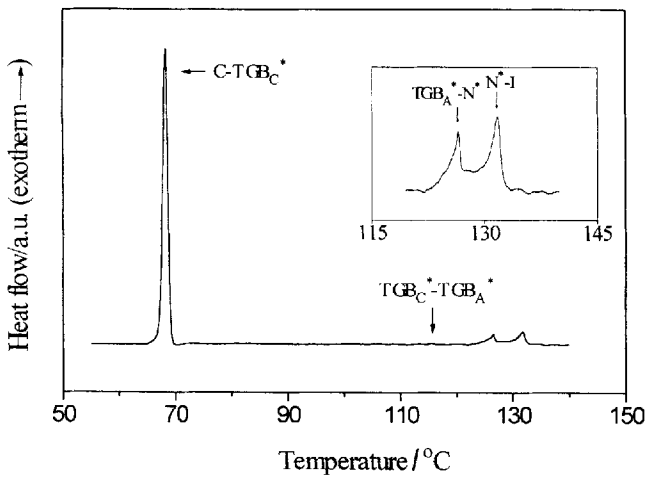

(*b*)

Figure 1. DSC thermogram for (*R,S*)P*m*PBNP. (*a*) $m=9$ and (*b*) $m=12$ on cooling.

rise of the S_A^*–S_C^* transition temperatures results in a decreasing thermal stability of the S_A^* phase which is then completely suppressed by the existence of TGB_A^* phase as m is extended to greater than 11. Surprising as it may seem, the thermal stabilities of the TGB_A^* phase are not significantly changed by increasing m from 11 to 14. The diagram also reveals that lengthening the alkyl chain from $m=7$ to 10 favours the formation of a ferroelectric S_C^* phase, and further lengthening m promotes the formation of the TGB_C^* phase.

Transition enthalpies were determined by DSC and are also summarized in the table. It is very difficult to obtain separate transition enthalpies of the N*–TGB_A^* and TGB_A^*–S_A^* transitions in the case of shorter alkyl chain length ($m=7$–10), since they so closely overlap as seen in figure 1. Thus, the enthalpies of both changes are summed and contained in the N*–TGB_A^* transition. The enthalpies of the S_A^*–S_C^* transition are not detectable in the DSC traces, however, the enthalpies of the TGB_A^*–TGB_C^* transitions, with the exception of $m=11$, are detectable but rather small. It seems that both the S_A^*–S_C^* and TGB_A^*–TGB_C^* transitions are of second order in nature.

3.2. *Microscopic observations*

Compounds (*R,S*)P*m*PBNP sandwich-packed between two untreated glass slides were carried out in the cooling and heating cycles for the microscopic observation of the textures. The N* phase appears in all members as characterized by the planar and paramorphotic textures. On cooling to the TGB_A^* phase, in the case of shorter alkyl chain length ($m=7$–10), the planar texture of the N* phase remains and simply selectively reflects the colour. However, the paramorphotic texture alters to a spiral shape of filaments accompanied with homeotropic (dark) S_A domain as shown as an example in figure 3 for $m=9$. This spiral filament texture does not resemble the *vermis* texture reported for most TGB_A^* substances [1, 4, 6, 7]. However, further investigation of the compounds packed in Cano wedge cells showed a texture of filament zones and Grandjean plane disclination lines, and in homogeneously aligned cells exhibited a cholesteric texture, demonstrating the existence of the TGB_A^* phase [7, 17]. Recently, a similar texture has been observed in a binary mixture of non-chiral with chiral substances in the TGB_A^* phase close to the TGB_C^* phase [18, 19]. Sprial filaments significantly reduce as the temperature decreases and completely disappear as the TGB_A^*–S_A^* transition occurs. Consequently, the S_A^* phase displays typical fan-shaped and homeotropic textures. As the temperature continues to cool down immediately after the S_A^* phase, striated fan-shaped and pseudo-homeotropic (dark) textures appear characteristic of the S_C^* phase. It is worth noting that the pseudo-homeotropic texture selectively reflects coloured light with changes in temperature; at lower temperatures the texture appears blue and at higher temperatures it appears red, as can be seen from figures 4(*a*) and (*b*), respectively. This texture is called the 'petal' texture [20], characteristic of the S_C^* phase, normally observed when the helix of the S_C^* phase is of a pitch such that iridescent light in the visible region of the spectrum is reflected.

Similar microphotographic textures of the TGB_A^* phase are also detected in the case of longer alkyl chain lengths ($m=11$–14), with the exception that the spiral filaments remained unchanged in the whole temperature range of the phase. It has to be pointed out that the textures of these homologues depend remarkably on the thickness of the samples prepared between two untreated

Table. Transition temperatures and enthalpies ΔH (in italics) of chiral compounds (*R,S*)p*m*PBNP on cooling

	T/°C and ΔH/kJ^{-1} mol^{-1} (in italics)															
m	I		N*		TGB_A^*			S_A^*		S_C^*/TGB_C^*			Cr		m.p.	
7	●	152·5	●	150·1	●	148·8[a]		●	98·0[a]	●	97·3		●	115·1		
		1·59		*0·54*		[b]			[c]		*37·85*			*39·84*		
8	●	147·9	●	146·4	●	143·7[a]		●	106·1[a]	●	84·1		●	109·1		
		1·67		*0·50*		[b]			[c]		*29·69*			*30·12*		
9	●	142·8	●	140·8	●	136·0[a]		●	105·9[a]	●	79·1		●	97·1		
		1·21		*1·09*		[b]			[c]		*17·46*			*18·32*		
10	●	139·4	●	136·6	●	131·0[a]		●	108·4[a]	●	66·9		●	89·5		
		1·14		*0·64*		[b]			*0·13*		*16·04*			*17·20*		
11	●	134·3	●	127·5	●				114·1[a]	●	73·7		●	85·5		
		1·17		*0·92*					[c]		*26·25*			*27·12*		
12	●	132·6	●	126·4	●				113·4[a]	●	69·0		●	82·6		
		1·21		*0·88*					*0·04*		*26·84*			*27·90*		
13	●	138·5	●	133·7	●				119·7[a]	●	68·6		●	83·8		
		1·38		*0·63*					*0·25*		*18·21*			*19·31*		
14	●	136·5	●	132·8	●				119·4[a]	●	71·1		●	80·5		
		1·93		*0·96*					*0·29*		*29·52*			*30·45*		

[a] The transition temperature was obtained by microscopic observation.
[b] The enthalpy of the TGB_A^*–S_A^* transition was added to the N*–TGB_A^* transition value.
[c] The enthalpy was too small to be measured by DSC.

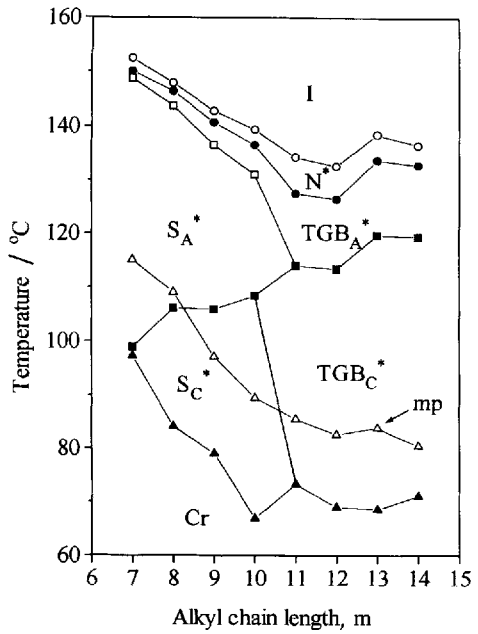

Figure 2. A plot of the transition temperatures as function of the alkyl chain length for (*R,S*)P*m*PBNP. ○, I–N*; ●, N*–TGB_A^*; □, TGB_A^*–S_A^*; ■, S_A^*–S_C^* or TGB_A^*–TGB_C^*; ▲, S_C^*–C or TGB_C–C; △, m.p.

glass slides. For example, the TGB_A^* texture may appear as coloured spiral filaments spread over most of the microphotographic domain as shown in figure 5 and remain nearly unchanged in the whole temperature range of the phase. As the temperature lowers immediately after the TGB_A^* phase, the texture displays not only coloured spiral filaments but are accompanied with striated disclination lines in certain areas as shown in figure 6. A similar texture has been observed by Shao *et al.* [3], and proposed as evidence of the existence of the TGB_C^* phase.

Furthermore, an interesting microscopic texture was found in the materials packed in 2 μm homogeneously aligned cells and cooled from the isotropic liquid without an applied electric field. The texture in the S_C^* and TGB_C^* phases exhibit two types of domain with different relative directions of the smectic layer normal as shown in figure 7 obtained for compound $m=9$. This texture has been reported by Komitov *et al.* [21], in some ferroelectric liquid crystal materials possessing the N*–S_C^* phase sequence and is called a parquet or stripe-like quasi-periodic texture. This parquet texture detected for longer chain members ($m=9$–14), illustrates that the formation of the texture has no connection with the origin of the S_A^*–S_C^* or TGB_A^*–TGB_C^* phase sequence. The occurrence of this texture may presumably be attributed to the nature of interaction between liquid crystal molecules and homogeneously aligned polyimides.

The results of the DSC study and the microscopic observations also clearly reveal that the TGB_A^* phase behaves differently and depends remarkably on the alkyl chain length. One can conclude that in the case of shorter chain length ($m \leqslant 10$), the TGB_A^* phase behaves in such a way as a metastable-like phase mediated between N* and S_A^* phases and thus appears in a shorter temperature range, whereas, that of longer chain length

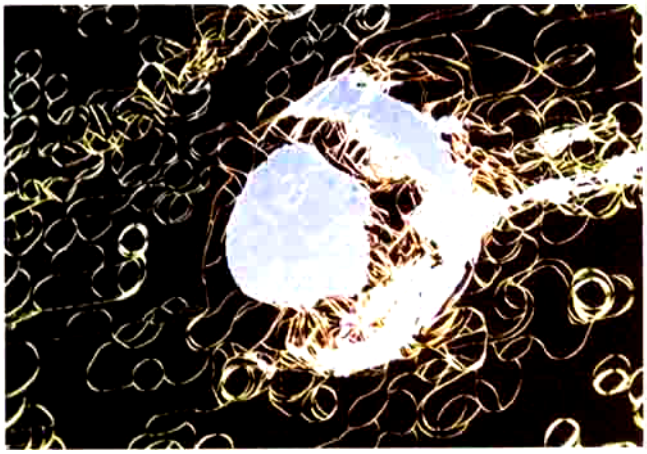

Figure 3. The planar and spiral filament textures of the TGB_A^* phase obtained for (*R,S*)P9PBNP under crossed polarizing microscopy at 139·8°C (magnification × 600).

(a)

(b)

Figure 4. The petal and striated fan-shaped textures of the S_C^* phase obtained for (*R,S*)P9PBNP under crossed polarizing microscopy at (*a*) 107·3°C and (*b*) 102·5°C (magnification × 600).

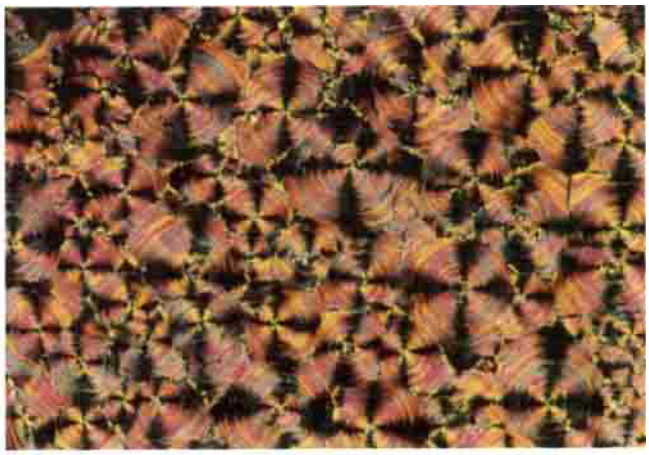

Figure 5. The coloured spiral filament texture of the TGB_A^* phase obtained for (*R,S*)P11PBNP under crossed polarizing microscopy at 120.2°C (magnification × 600).

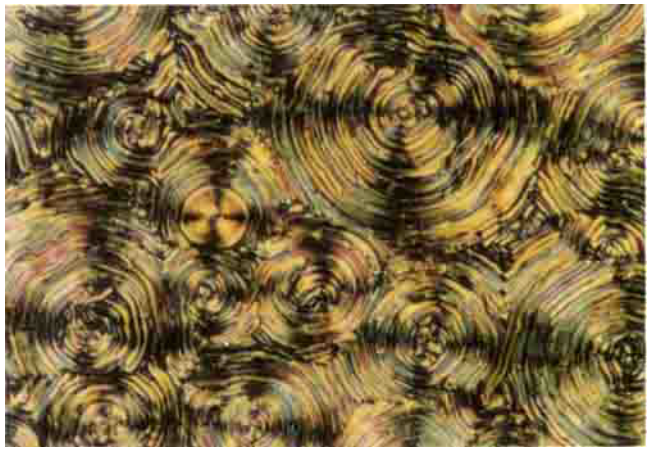

Figure 6. The coloured spiral filament texture with striated disclination lines of the TGB_C^* phase obtained for (*R,S*)P11PBNP under crossed polarizing microscopy at 108·1°C (magnification × 1200).

Figure 7. The parquet texture of the S_C^* phase in the homogeneous alignment cell with 2 μm thickness obtained for (*R,S*)P9PBNP under crossed polarizing microscopy at 111·6°C (magnification × 150).

($m \geqslant 11$), TGB_A^* phase behaves as a thermodynamically stable phase and consequently exists in a wider temperature range.

3.3. *Spontaneous polarization*

The magnitudes of the spontaneous polarization (P_S) for all materials were measured as a function of temperature in 2 μm homogeneously aligned cells. It is noted [3] that both the TGB_A^* and TGB_C^* phases could be converted to normal S_A^* and S_C^* phases by the application of an electric field resulting in electroclinic and ferroelectric switching, respectively. Examples obtained for compounds related to two different Curie points: $T_{S_A^*-S_C^*}$ (m = 8, 9) and $T_{TGB_A^*-TGB_C^*}$ (m = 12) recorded at the frequency of 100 Hz and amplitude of 38·5 V_{p-p} are shown in figure 8. It is clearly shown that the P_s values are nearly identical at the same temperature below the Curie points. Moreover, the magnitudes of spontaneous polarization

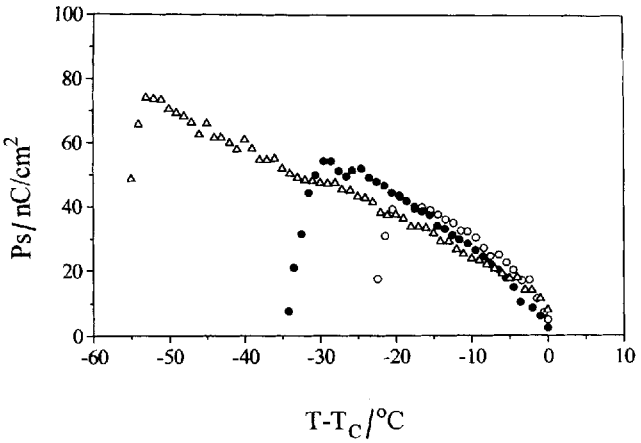

Figure 8. Magnitude of the spontaneous polarization plotted as a function of temperature for (*R,S*)P*m*PBNP. ○, m = 8; ●, m = 9; △, m = 12.

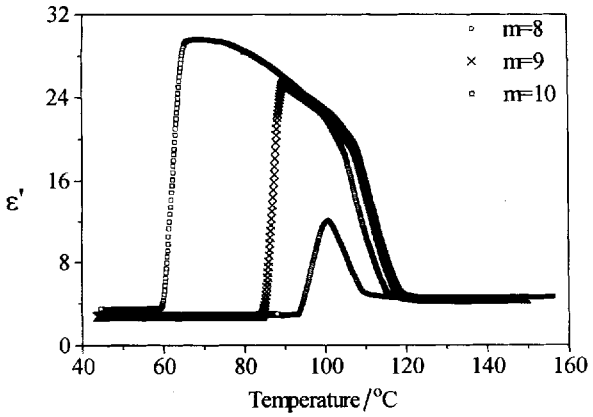

Figure 9. Temperature dependence of dielectric constant ε′ of (*R,S*)P*m*PBNP (m = 8–10) at 1 KHz. ○, m = 8; x, m = 9; □, m = 10.

are evidently independent of the nature of the S_A^*–S_C^* or TGB_A^*–TGB_C^* transitions.

3.4. *Dielectric properties*

The real part of the dielectric constant ε′ measured as a function of the temperature (on cooling) for some

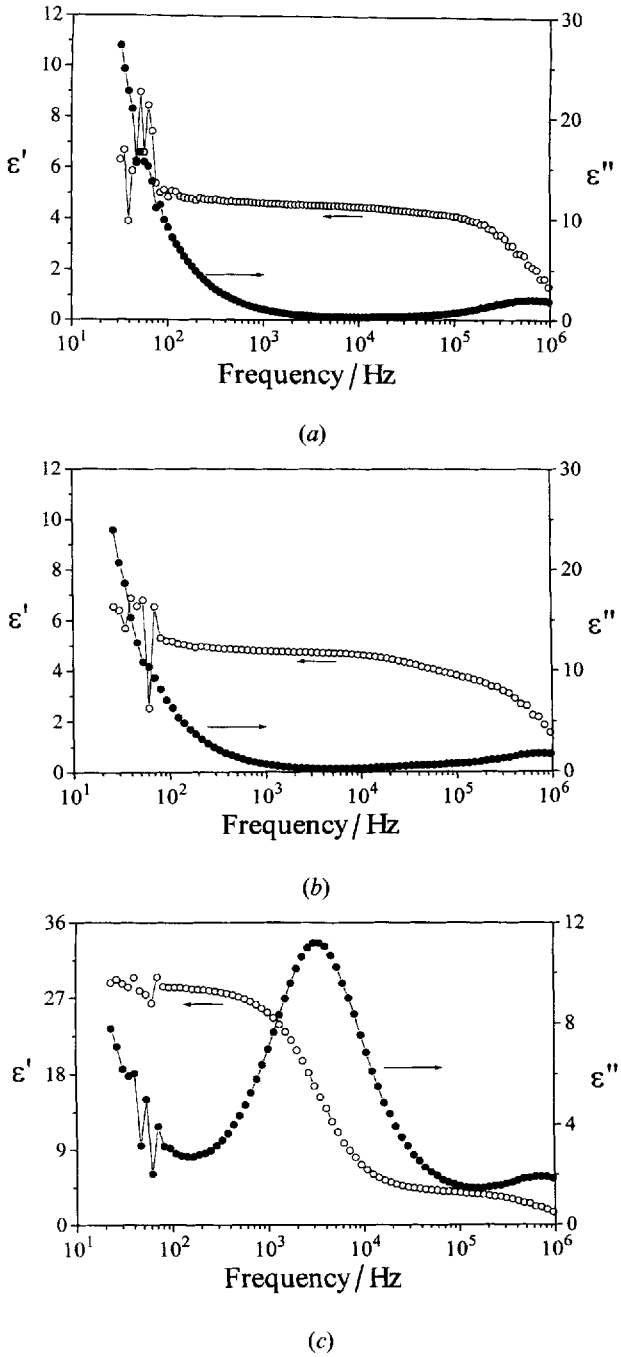

Figure 10. Some representative dispersion curves of (*R,S*)P10PBNP, plotted as ε′ and ε″ versus frequency in (*a*) the TGB_A^* phase at 134·2°C, (*b*) the S_A^* phase at 122·2°C and (*c*) the S_C^* phase at 93·7°C.

representative compounds ($m=8$–10) at a frequency of 1 kHz is plotted in figure 9. Sharp phase transitions of the S_A^* to the corresponding S_C^* phase can be clearly seen from the dispersion curves. Interestingly, the results also indicate that the dielectric constant in the TGB_A^* phase appears nearly the same as that in S_A^* phase, and suggests that the TGB_A^* phase has a low dipole polarization in the applied electric field.

More detailed macro- and micro-molecular motions of molecules in the mesophases investigated by frequency-dependent dielectric measurements for compound (*R,S*)P10PBNP are presented in figures 10(*a*)–(*c*). Figure 10(*a*) refers to the dispersion curves of (*R,S*)P10PBNP in the TGB_A^* phase at 134·2°C. The real part ε' is not stable at low frequency but it keeps nearly flat at about 4·8 between 100 Hz and 10 kHz, indicating no significant occurrence of the relaxation process in the TGB_A^* phase. The dispersion curves of figure 10(*b*) measured in the S_A^* phase at 122·2°C show that the real part ε' keeps nearly flat at about 4·5 between 100 Hz and 10 kHz. Around 10 kHz, they show a drop of ε' and a loss of peak ε'', probably resulting from a soft mode tilt fluctuation [22]. Figure 10(*c*) shows the dispersion curves in the S_C^* phase at 93·7°C. The ε' reaches about 27 at low frequency and drops to about 4 at 10 kHz, and a loss peak of ε'' appears at the relaxation frequency around 3 kHz. This feature may result from a Goldstone mode phase fluctuation [22].

4. Conclusions

A new series of chiral compounds (*R,S*)P*m*PBNP ($m=7$–14) has been demonstrated to exhibit two frustrated phases: TGB_A^* and TGB_C^*. Moreover, the stability of these phases depends remarkably on the nature of the alkyl chain length *m*; as $m \leqslant 10$, the TGB_A^* phase behaves as a metastable-like phase, whereas, as $m \geqslant 11$, both the TGB_A^* and TGB_C^* phases become thermodynamically stable. Consequently, this series of chiral materials results in two distinguishable phase sequences: N*–TGB_A^*–S_A^*–S_C^* and N*–TGB_A^*–TGB_C^*.

References

[1] Goodby, J. W., Waugh, M. A., Stein, S. M., Chin, E., Pindak, R., and Patel, J. S., 1989, *J. Am. chem. Soc.*, **111**, 8119.

[2] Nguyen, H. T., Bouchta, A., Navailles, L., Barois, P., Isaert, N., Twieg, R. J., Maaroufi, A., and Destrade, C., 1992, *J. Phys. II (France)*, **2**, 1992.

[3] Shao, R. F., Pang, J. H., Clark, N. A., Rego, J. A., and Walba, D. M., 1993, *Ferroelectrics*, **147**, 255.

[4] Slaney, A. J., and Goodby, J. W., 1991, *J. mater. Chem.*, **1**, 5.

[5] Slaney, A. J., and Goodby, J. W., 1991, *Liq. Cryst.*, **9**, 849.

[6] Nguyen, H. T., Twieg, R. J., Nabor, M. F., Isaert, N., and Destrade, C., 1991, *Ferroelectrics*, **121**, 187.

[7] Booth, C. J., Dunmur, D. A., Goodby, J. W., Kang, J. S., and Toyne, K. J., 1994, *J. mater. Chem.*, **4**, 747.

[8] Dierking, I., Gieelmann, F., and Zugenmaier, P., 1994, *Liq. Cryst.*, **7**, 17.

[9] Werth, M., Nguyen, H. T., and Destrade, C., 1994, *Liq. Cryst.*, **17**, 863.

[10] Nguyen, H. T., Destrade, C., Parneix, J. P., Pochat, P., Isaert, N., and Girold, C., 1993, *Ferroelectrics*, **147**, 181.

[11] Goodby, J. W., Slaney, A. J., Booth, C. J., Nishyama, I., Vuijk, J. D., String, P., and Toyne, K. J., 1994, *Mol. Cryst. liq. Cryst.*, **243**, 231.

[12] Miyasato, K., 1983, *Jap. J. appl. Phys.*, **22**, L661.

[13] Wu, S.-L., Chen, D.-G., Hsieh, W.-J., Yu, L.-J., and Liang, J.-J., 1994, *Mol. Cryst. liq. Cryst.*, **250**, 153.

[14] Hiraoka, K., Tagukchi, A., Ouchi, Y., Takezoe, H., and Fukuda, A., *Jap. J. appl. Phys.*, **29**, L103 (1990).

[15] De Gennes, P. G., 1972, *Sol. St. Comm.*, **10**, 753.

[16] Renn, S. R., and Lubensky, T. C., 1988, *Phys. Rev. A*, **38**, 2132.

[17] Isaert, N., Navvilles, L., Barois, P., and Nguyen, H. T., 1994, *J. Phys. II (France)*, **4**, 1501.

[18] Kuczyanski, W., and Stegemeyer, H., 1994, *Ber. Bunnsenges. phys. Chem.*, **98**, 1322.

[19] Kuczyanski, W., and Stegemeyer, H., 1995, *Mol. Cryst. liq. Cryst.*, **260**, 377.

[20] Gray, G. W., and McDonnel, D. G., 1976, *Mol. Cryst. liq. Cryst.*, **37**, 189.

[21] Komitov, L., Lagerwall, S. T., Matuszczyk, M., Stebler, B., Gruneberg, K., and Scherowsky, G., 1995, *Ferroelectrics*, in press.

[22] Gouda, F., Skarp, K., and Lagerwall, S. T., 1991, *Ferroelectrics*, **113**, 165.